

Avalanche Dynamics in Wet Granular Materials

P. Tegzes,^{1,2} T. Vicsek,² and P. Schiffer^{1,*}

¹*Department of Physics and Materials Research Institute,
Pennsylvania State University, University Park PA 16802*

²*Department of Biological Physics, Eötvös Loránd University, 1A Pázmány stny., Budapest, Hungary 1117*
(Dated: October 30, 2018)

We have studied the dynamics of avalanching wet granular media in a rotating drum apparatus. Quantitative measurements of the flow velocity and the granular flux during avalanches allow us to characterize novel avalanche types unique to wet media. We also explore the details of viscoplastic flow (observed at the highest liquid contents) in which there are lasting contacts during flow, leading to coherence across the entire sample. This coherence leads to a velocity independent flow depth at high rotation rates and novel robust pattern formation in the granular surface.

PACS numbers: 45.70.-n, 45.70.Ht, 45.70.Mg

Avalanches and landslides [1, 2, 3] are among the most dramatic of natural catastrophes, and they also provide an evocative metaphor for a wide range of propagating breakdown phenomena from impact ionization in semiconductors [4] to magnetic vortex motion in superconductors [5]. On the other hand, the existence of avalanches, i.e. the sudden collapse of the system previously frozen into a high energy state, is a fundamental manifestation of the metastable nature of granular materials. Studies of avalanches [6, 7, 8] and surface flows [9] in granular media have largely focused on dry grains. By wetting such media, however, one introduces controllable adhesive forces between the grains [10, 11] which lead to qualitatively new behavior [12, 13, 14, 15, 16, 17, 18]. In our previous work [13] we identified three fundamental regimes for the repose angle of wet granular materials as a function of the liquid content. The granular regime at very low liquid contents is dominated by the motion of individual grains; in the correlated regime corresponding to intermediate liquid contents, a rough surface is formed by the flow of separated clumps; and the repose angle of very wet samples results from cohesive flow with viscoplastic properties.

Here we report investigations of the avalanche dynamics and flow properties of wet granular materials, employing a rotating drum apparatus (a cylindrical chamber partly filled with a granular medium and rotated around a horizontal axis) [6, 7]. At low rotation rates, the medium remains at rest relative to the drum while its surface angle is slowly increased by rotation, up to a critical angle (θ_{max}) where an avalanche occurs, thus decreasing the surface angle to the repose angle (θ_r). The flow becomes continuous at high rotation rates, but the transition between avalanching and continuous flow is hysteretic in rotation rate in dry media [6, 19].

Previous studies of cohesive granular media in a rotating drum [15, 16, 17] have focused on the surface angles of the medium before and after avalanches. For example, Quintanilla *et al.* recently performed a statistical analysis of avalanche size based on these angles, and showed

that the average clump size increased with cohesion [20]. In our measurements, we focus instead on characterizing the *dynamics of cohesive flow*. We quantitatively investigate the flow dynamics during avalanches at different liquid contents by analyzing the time evolution of the averaged surface profile obtained from hundreds of avalanche events, and we also measure surface velocities during continuous flow. In particular, we explore the nature of the viscoplastic flow, which displays unique characteristics associated with coherent motion over the entire granular surface.

We studied glass spheres thoroughly mixed with small quantities of hydrocarbon oil [21] varying between $\tau = 0.001\%$ and 5% of the void volume. In this regime the flow of oil due to gravity can be neglected. The inner diameter of our drum was 16.8 cm, its width was 3.2 cm, and the granular filling was 30%. Measurements performed in a thinner (2 cm) drum verified that wall effects do not modify the qualitative behavior. We studied two different sizes of beads ($d_1 = 0.5\text{ mm} \pm 20\%$ and $d_2 = 0.9\text{ mm} \pm 11\%$), and the results were qualitatively equivalent in the two cases except where noted otherwise. The experiment was recorded by a CCD video camera interfaced to a computer which could analyze the spatiotemporal evolution of the surface profile (height variations in the axial direction were negligible). To determine the position of the surface, we used background illumination and an algorithm based on local contrast which gave us a resolution of $\delta t = 0.03$ seconds and $\delta x = 0.5$ mm.

Surface angles. — We first investigated the avalanching – continuous flow transition for various liquid contents. We slowly increased and then decreased the rotation rate and measured the average surface angles, θ_{max} and θ_r in the avalanching regime. We consider the flow continuous when the medium never comes to rest with respect to the drum, which coincides with $\Delta\theta \equiv \theta_{max} - \theta_r < 1^\circ$. The results of typical runs are presented in Fig. 1 (a), (b) and (c), where θ_{max} and θ_r are plotted as a function of the rotation rate.

The three basic types of behavior observed previously

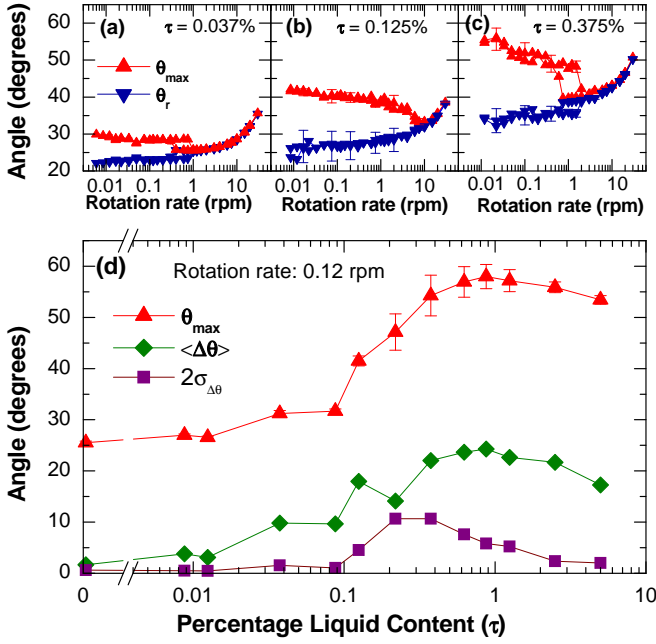


FIG. 1: (a) (b) (c) θ_{max} and θ_r as a function of rotation rate for 3 different liquid contents. The error bars represent the standard deviation of the observed angle distributions. (d) The maximum angle, θ_{max} , the average avalanche size, $\langle\Delta\theta\rangle$, and the width of the avalanche size distribution $2\sigma_{\Delta\theta}$ as a function of liquid content. (The data were taken using small beads, $d = 0.5$ mm)

are also reflected in the present experiment. In the granular regime at low liquid contents, (e.g. $\tau = 0.04\%$), the behavior is qualitatively similar to the dry case, and we observe a clear hysteretic transition between continuous flow and avalanching (Fig. 1 (a)). At a somewhat higher liquid content ($\tau = 0.125\%$, see Fig. 1 (b)) the correlated behavior is marked by a lack of hysteresis, and avalanching behavior is observed at a relatively high rotation rate compared to the other regimes. The continuous flow in this regime consists of a stream of separated clumps rather than the constant flux seen in the other two regimes. At $\tau = 0.375\%$ (Fig. 1 (c)) hysteresis is again observed, reflecting the onset of the viscoplastic continuous flow, which is smooth and coherent over the entire sample.

An interesting feature of the curves in Fig. 1 (a-c), is that θ_{max} decreases with increasing rotation rate, although at slow rotation (where the rotation of the drum during the avalanche is negligible) the rotation rate influences the avalanche process only through changes in the waiting time between successive avalanches. We find that θ_{max} depends logarithmically on this waiting time [25], reminiscent of other granular aging phenomena [15, 22]. The effect is more pronounced at higher liquid contents, and we attribute it to the motion of liquid flowing towards the contact points rather than condensation effects [15] since the vapor pressure of the oil is low.

If the rotation rate is sufficiently low, then discrete avalanches occur at all liquid contents. In the following paragraphs we analyze this avalanching regime. Fig. 1 (d) shows $\langle\theta_{max}\rangle$ (averaged over several hundred avalanches) as a function of liquid content. The distribution is close to Gaussian, and the error bars in the figure indicate the standard deviation. The average avalanche size $\langle\Delta\theta\rangle = \langle\theta_{max} - \theta_r\rangle$ and the width of the avalanche size distribution $2\sigma_{\Delta\theta} = 2(\langle\Delta\theta^2\rangle - \langle\Delta\theta\rangle^2)^{1/2}$ are also plotted in Fig. 1 (d). We interpret these results below in the context of a more detailed investigation of the avalanche dynamics.

Flow Dynamics. — By using the rotating drum apparatus, we can obtain information not just about the medium before and after the avalanche events, but we can also study the details of the grain motion *during avalanche events*. In order to analyze the dynamics of avalanches we have obtained two dimensional space-time matrices, $h(x, t)$, characterizing the sample surfaces throughout the avalanche process which can then be analyzed to produce a variety of information about the individual avalanches. By taking derivatives of the $h(x, t)$ data, we obtain the local angle ($\alpha(x, t) = \arctan[\partial_x h(x, t)]$) and the local vertical velocity ($u(x, t) = \partial_t h(x, t)$) of the surface profile. Furthermore, by then integrating the vertical velocity (using the continuity equation and assuming constant density [23]), we also obtain the local flux in the avalanche, i.e. $\phi(x, t) = \rho w \int_{-D/2}^x \partial_t h(x', t) dx'$ (where ρ is the grain density, w is the width of the drum, and D is the drum diameter), which represents the material flowing through a given vertical plane at position x .

In Fig. 2 (a) we present snapshots of the progression of single avalanches for several typical liquid contents. Fig. 2 (b) displays $\alpha(x, t)$ as a function of space (horizontally) and time (downwards) for the same individual avalanches. In Fig. 2 (c-e), we present the average behavior of 300-500 avalanches at the same liquid contents, and show similar graphs of the time evolution of $\langle\alpha(x, t)\rangle$, $\langle u(x, t)\rangle$, and $\langle\phi(x, t)\rangle$, where $\langle\rangle$ denotes averaging over avalanches. By obtaining these quantitative measures of the averaged properties, we can separate the robust characteristics of the avalanche dynamics from the large fluctuations which are inherent in avalanche processes.

In the avalanches among dry grains [6, 7, 8], the avalanches consist of flow in a thin layer near the smooth surface and have a much longer duration and much smaller flux than in the wet media. The size of the avalanches is $\Delta\theta \approx 2^\circ \pm 0.5^\circ$. At low but nonzero liquid contents (e.g. $\tau = 0.04\%$) θ_{max} and $\Delta\theta$ become larger due to the onset of intergrain cohesion. In this granular regime the avalanche is initiated by a front traveling downhill (bright line in Fig. 2 (c)), but we can also observe a second front traveling uphill (dark line). The second front is also apparent in the motion of the point of maximum flux, Fig. 2 (e), and it corresponds to the

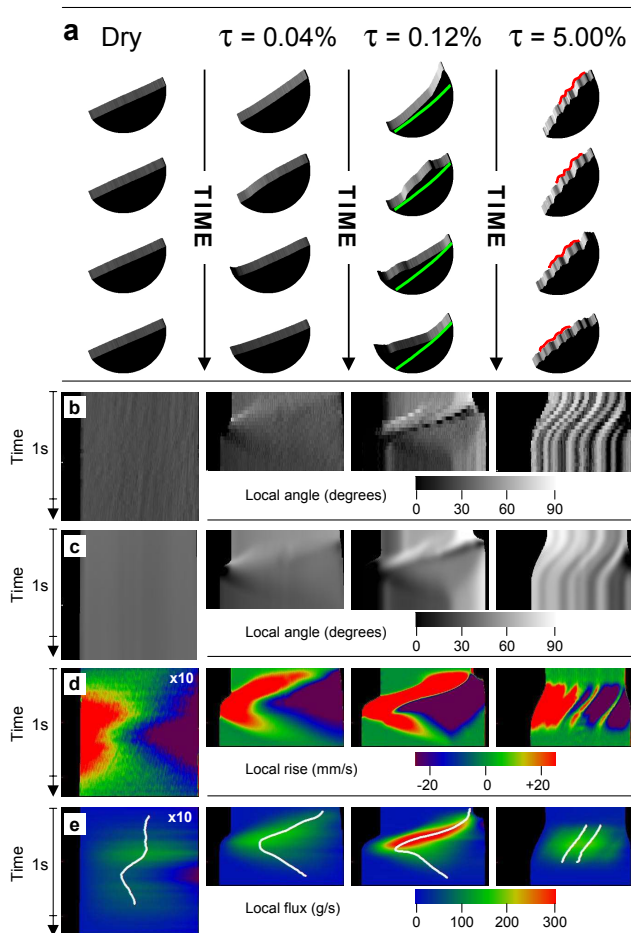


FIG. 2: Dynamics of avalanches of different types with grain size $d = 0.5$ mm. (a) Snapshots (at 0.1–0.2 s time intervals) of four single avalanches corresponding to different liquid contents. The third dimension is used for a brightness-coded representation of the local slope (α). The green lines indicate approximate slip planes in the correlated regime, and the red line shows the traveling quasi-periodic surface features in the viscoplastic regime. (b) The local slope with the same brightness coding, as a function of space and time. A horizontal line corresponds to a surface profile at a given instant, and time propagates downwards (thus avalanches propagate leftwards and down). The stripes indicate lasting surface features. (c) (d) (e) The characteristic features of the avalanches averaged over several hundred independent avalanches. The displayed quantities are: (c) local surface angle, (d) the rate of change of local height, and (e) the local grain flux (the white lines indicate the point of maximum current). Note that the surface patterns at the highest liquid contents are robust against averaging. The standard deviations of the averaged data sets were typically 5 – 25 % of the mean value. In some cases, however, the noise originating from taking numerical derivatives leads to standard deviations comparable to the mean. For this reason averaging over several hundred independent events was absolutely necessary, resulting in standard errors ranging from 0.2 – 6 %.

grains reaching a solid barrier at the bottom [24].

At intermediate liquid contents (the correlated regime, $0.1\% \lesssim \tau \lesssim 0.5\%$), both θ_{max} and $\Delta\theta$ increase substantially. In this regime, the principal failure mechanism is a fracture along a curved slip plane (approximated by the green lines in Fig. 2 (a)), analogous to the dynamics of a class of geological events known as “slides” [2]. In the figure there is a single slip plane, which leads to large avalanches with a relatively narrow distribution. However, at larger liquid contents the avalanches occur through a succession of local slip events followed by a large avalanche extending over the whole surface [25]. This leads to large fluctuations in the size of the avalanches (see Fig. 1 (d)) as observed in cohesive powders [20]. The medium becomes more cohesive with increasing liquid content, and the upward traveling front disappears for $\tau \geq 0.2\%$ since the material moving as a connected block stops coherently when it hits the bottom.

At the highest liquid contents, $\tau \approx 0.5 - 1\%$, the onset of coherent viscoplastic flow is apparent through numerous qualitative changes in the dynamics of flow. The coherence of avalanche flow in this regime is demonstrated by the parallel lines during the avalanche in Fig 2 (b) and (c). This behavior is qualitatively similar to a different class of geological event, called a “debris flow” or “mudflow” [2, 3]. Since the whole surface moves coherently (rather than breaking apart and evolving separately in different parts of the surface), fluctuations are strongly suppressed [13] and the avalanche size distribution is rather narrow (Fig. 1 (d)). The small decrease in θ_{max} is probably due to lubrication [13].

A novel property of the viscoplastic avalanches is the topology of the top surface which spontaneously forms a nearly periodic pattern (seen in Fig. 2 (a) and (b)). This surface structure is maintained essentially intact during the avalanche, indicating that there are lasting contacts in the flowing layer. Moreover, the same pattern in the surface features is reproduced at the end of each avalanche. This is demonstrated most clearly in Fig 2 (c), where the average of 347 avalanches of the $\tau = 5\%$ sample has the same features as the typical individual avalanche shown in Fig. 2 (a) and (b). The robust nature of the surface structure of the wettest grains is in sharp contrast to the other regimes where averaging completely smoothes out the smaller surface features. We can understand this behavior as resulting from coherence of the entire flow, which strongly reduces fluctuations in this regime. With minimal fluctuations, the final surface structure after each avalanche is essentially the same, thus setting the same initial condition for the next avalanche. With the same initial conditions for each avalanche, naturally the surface features are reproduced each time. Our experiments with the larger ($d = 0.9$ mm) beads also revealed pattern formation, but with a smaller characteristic size corresponding to 8-10 grain diameters.

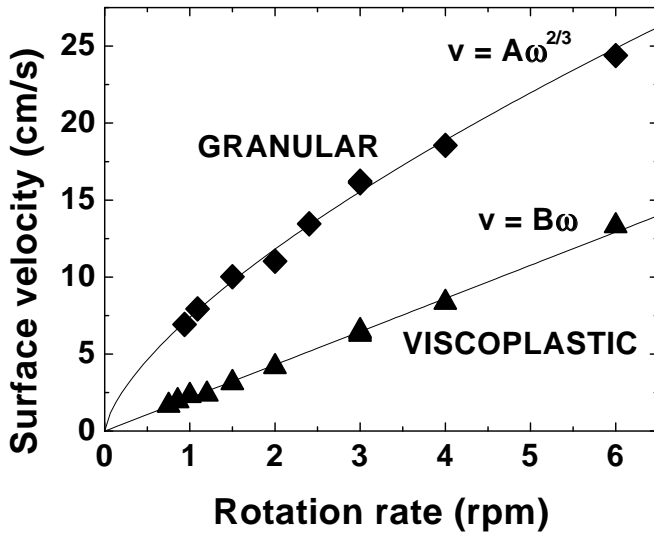


FIG. 3: The surface velocity v during continuous flow as a function of rotation rate ω for dry grains and in the viscoplastic regime, $\tau = 5\%$ (large beads, $d = 0.9$ mm). The continuous lines represent power-law fits to the data. The linear behavior for the viscoplastic flow indicates that flow depth is independent of the rotation rate.

The difference is probably due to the smaller ratio of the cohesive forces to the gravitational forces on the grains.

In addition to differences in the avalanching behavior, the viscoplastic regime also displays continuous flow which is rather different from that at lower liquid contents. We compare the viscoplastic and granular continuous flows by measuring their surface velocities v (by means of tracer particles) as a function of rotation rate in Fig. 3 (continuous flow is only observed in the correlated regime above 6 rpm, and we therefore do not include data from that regime here). For these measurements we used the larger, ($d = 0.9$ mm) beads. The viscoplastic flow is slower than the granular flow by a factor of two, and the two curves correspond to rather different functional forms. The curvature in the granular case suggests that the flow depth increases with rotation rate as previously suggested [26]. The linear $v(\omega)$ function of the viscoplastic flow suggests a *constant flow depth* which is independent of the flow rate. This observation is consistent with the coherent nature of the flow: the flow depth is not determined by local mechanisms, but is fixed by the geometry of the whole system [9].

Discussion. — While the flows we observe appear to have analogies with geological events, it is important to note that real geological materials usually consist of polydisperse irregular particles often with very high ($\tau \approx 100\%$) water contents and that the scaling of our system to geological lengthscales is non-trivial. Furthermore, avalanche studies in real soil have demonstrated additional phenomena associated with soil saturation [27]. Interestingly we still recover some of the

basic dynamical processes in our model system, which constitutes an important step towards the description of qualitatively different flow behaviors in the framework of a single model [17, 28]. The changes in the dynamical behavior with wetting are associated with the increasingly coherent nature of the flow, i.e. the formation of coherently moving clusters – clumps – due to the increased cohesion and viscous effects. Within a cluster, local velocity fluctuations should be suppressed, and thus the local granular temperature ($T = \langle v^2 \rangle - \langle v \rangle^2$) should approach zero, but the clusters themselves both form and break apart during an avalanche process in a finite container. An important theoretical question raised by our data is how a length scale describing the size of the clumps may emerge from a granular flow model, and how such a length scale would vary with the type of media, the nature of intergranular adhesion, and the type of granular flow.

We gratefully acknowledge helpful discussions with J. Banavar, A.-L. Barabási, and Y. K. Tsui. We are also grateful for support from the Petroleum Research Fund and the NASA Microgravity Fluid Physics Program. P. T. and T. V. are grateful for the partial support from OTKA Grant No. T033104.

* Electronic address: schiffer@phys.psu.edu

- [1] E. E. Brabb and B. L. Harrod (eds.), *Landslides: Extent and Economic Significance* (Balkema, Rotterdam, 1989).
- [2] R. Dikau, D. Brunsden, L. Schrott, and M.-L. Ibsen, *Landslide Recognition* (Wiley, Chichester, 1996) (see appendix 2 for classification of types of avalanches).
- [3] R. M. Iverson, *Rev. Geophys.*, **35**, 245 (1997); P. Coussot, *Mudflow rheology and dynamics* (A.A. Balkema, Rotterdam, 1997).
- [4] W. Clauss, A. Kittel, U. Rau, J. Parisi, J. Peinke, and R.P. Huebener, *Europhys Lett.* **12**, 423 (1990).
- [5] S. Field, J. Witten, F. Nori, and X. Ling, *Phys. Rev. Lett.* **74**, 1206 (1995).
- [6] J. Rajchenbach, *Phys. Rev. Lett.* **65**, 2221 (1990).
- [7] C.-h. Liu, H. M. Jaeger, and S. R. Nagel, *Phys. Rev. A* **43**, 7091 (1991).
- [8] H. M. Jaeger, Liu, C.-h., and S. Nagel, *Phys. Rev. Lett.* **62**, 40 (1989); A. Daerr and S. Douady, *Nature* **399**, 241 (1999); M. Bretz, J. B. Cunningham, P. L. Kurczynski, and F. Nori, *Phys. Rev. Lett.* **69**, 2431 (1991); V. Frette *et al.*, *Nature* **379**, 49 (1996).
- [9] K. Yamane, M. Nakagawa, S. A. Altobelli, T. Tanaka, and Y. Tsuji, *Phys. Fluids* **10**, 1419 (1998); P.-A. Lemieux and D.J. Durian, *Phys. Rev. Lett.* **85**, 4273 (2000); T. S. Komatsu, S. Inagaki, N. Nakagawa, and A. Nasuno, *Phys. Rev. Lett.* **86**, 1757 (2001).
- [10] H. Schubert *Powder Tech.* **37**, 105 (1984).
- [11] R. F. Craig *Soil Mechanics* (6th edition, E & FN Spon, New York, 1997).
- [12] D. J. Hornbaker, R. Albert, I. Albert, A.-L. Barabási, and P. Schiffer, *Nature* **387**, 765 (1997).

- [13] P. Tegzes, R. Albert, M. Paskvan, A.-L. Barabási, T. Vicsek, and P. Schiffer, *Phys Rev E*. **60**, 5823 (1999).
- [14] T. C. Halsey and A. J. Levine, *Phys Rev. Lett.* **80**, 3141 (1998); T. G. Mason, A. J. Levine, D. Ertas, and T. C. Halsey, *Phys. Rev. E* **60**, 5044 (1999).
- [15] L. Bocquet, E. Charlaix, S. Ciliberto, and J. Crassous, *Nature* **396**, 735 (1998).
- [16] N. Fraysse, H. Thomé, and L. Petit, *European Phys. J. B* **11**, 615 (1999).
- [17] S. T. Nase, W. L. Vargas, A. A. Abatan, and J. J. McCarthy *Powder tech.* **116**, 214 (2001).
- [18] A. Samadani and A. Kudrolli, *Phys. Rev. Lett.* **85**, 5102 (2000).
- [19] Caponeri, C., S. Douady, S. Fauve, and S. Laroche, In E. Guazelli and L. Oger (Eds.), *Mobile Particulate Systems*, Kluwer, Dordrecht (1995) pp. 331.
- [20] M. A. S. Quintanilla, J. M. Valverde, A. Castellanos, and R. E. Viturro, *Cohesive Phys. Rev. Lett.* **87**, 194301 (2001).
- [21] The viscosity of the oil used was 0.27 poise, and its surface tension was 2×10^{-4} J/cm².
- [22] W. Losert, J.-C. Géminard, S. Nasuno, and J. P. Gollub, *Phys. Rev. E* **61**, 4060 (2000).
- [23] S. Douady, B. Andreotti, and A. Daerr, *Euro. Phys. J. B* **11**, 131 (1998).
- [24] H. A. Makse, S. Havlin, P. R. King, and H. E. Stanley, *Nature* **386**, 379 (1997).
- [25] P. Tegzes, P. Schiffer, and T. Vicsek, unpublished.
- [26] Naturally in our finite setup the flow depth cannot increase infinitely which may explain why our measured $v(\omega)$ deviates from $\omega^{1/2}$ which would be expected from a linear velocity profile. [9]
- [27] R. M. Iverson, M. E. Reid, N. R. Iverson, R. G. LaHusen, M. Logan, J. E. Mann, and D. L. Brien, *Science* **290**, 513 (2000) and references therein.
- [28] J. M. N. T. Gray, *J. Fluid Mech.* **441** 1 (2001).